

β -BaB₂O₄ deep UV monolithic walk-off compensating tandem

J. Friebe^a, K. Moldenhauer^a, E.M. Rasel^a, W. Ertmer^a,
L. Isaenko^b, A. Yelisseyev^b, and J.-J. Zondy^{c,*}

^a*Institut für Quantenoptik, Universität Hannover, Welfengarten 1, D-30167 Hannover, Germany.*

^b*The Branch of the Institute of Mineralogy and Petrography, SB RAS, 43 Russkaya St., RU-630058 Novosibirsk, Russia.*

^c*Institut National de Métrologie, CNAM, 292 rue Saint-Martin, F-75003, Paris, France.*

Abstract

The generation of watt-level cw narrow-linewidth sources at specific deep UV wavelengths corresponding to atomic cooling transitions usually employs external cavity-enhanced second-harmonic generation (SHG) of moderate-power visible lasers in birefringent materials. In this work, we investigate a novel approach to cw deep-UV generation by employing the low-loss BBO in a monolithic walkoff-compensating structure [Zondy *et al.*, J. Opt. Soc. Am. B **20** (2003) 1675] to simultaneously enhance the effective nonlinear coefficient while minimizing the UV beam ellipticity under tight focusing. As a preliminary step to cavity-enhanced operation, and in order to apprehend the design difficulties stemming from the extremely low acceptance angle of BBO, we investigate and analyze the single-pass performance of a $L_c = 8$ mm monolithic walk-off compensating structure made of 2 optically-contacted BBO plates cut for type-I critically phase-matched SHG of a cw $\lambda = 570.4$ nm dye laser. As compared with a bulk crystal of identical length, a sharp UV efficiency enhancement factor of 1.65 has been evidenced with the tandem structure, but at ~ -1 nm from the targeted fundamental wavelength, highlighting the sensitivity of this technique when applied to a highly birefringent material such as BBO. Solutions to angle cut residual errors are identified so as to match accurately more complex periodic-tandem structure performance to any target UV wavelength, opening the prospect for high-power, good beam quality deep UV cw laser sources for atom cooling and trapping.

Key words: UV cw second-harmonic generation, type-I monolithic walkoff-compensation, UV atom cooling and trapping.

PACS: 42.65.Ky;42.79.Nv;42.70.Mp

1 Introduction

The generation of watt-level range deep UV ($\lambda \leq 350$ nm) cw coherent radiation from second-harmonic generation (SHG) has been until now hampered by the lack of sufficiently transparent or phase-matchable nonlinear materials in the deep UV spectral range. Typically several hundreds milliwatt of deep UV radiation are required for the laser cooling and trapping of atomic optical clock species such as H, Mg, Hg, Be or Ag [1], due to the large saturation intensities of their cooling transition line. For instance, given the saturation intensities of the $^2S_{1/2}$ - $^2P_{3/2}$ transition in Ag ($\lambda = 328.1$ nm, $I_{\text{sat}} = 87$ mW/cm²), decelerating a thermal beam by use of a Zeeman slower and realizing a 3D magneto-optical trap (MOT) with sufficiently high atomic densities would require ~ 300 mW of UV power. In the first cooling and trapping attempt with Ag, only 40mW of UV radiation were available from the SHG of a red dye laser with LBO, impeding hence their capture from a thermal atomic beam and resulting in a low number of trapped atoms ($N_{\text{at}} = 3 \times 10^5$) loaded from background pressure [2]. Increasing the number of trapped atoms would improve the signal-to-noise ratio of the Hz-level linewidth $^2S_{1/2}$ - $^2D_{5/2}$ two-photon clock transition in Ag, that has been recently observed in a thermal beam Doppler-free two-photon spectroscopy experiment [3]. A large number of trapped atoms also increases the intrinsic stability of optical clocks based on neutral atoms. For Mg and Be atoms, the saturation intensities of the 1S_0 - 1P_1 cooling transition ($\lambda = 285.2$ nm for Mg and $\lambda = 234.9$ nm for Be) is even higher ($I_{\text{sat}} = 455$ mW/cm² for Mg and $I_{\text{sat}} = 1097$ mW/cm² for Be) [4]. For the Mg clock experiment running in Hannover, only 100 mW of UV is presently available from the external cavity-enhanced SHG of a dye laser using a bulk BBO crystal. The large walkoff angle of BBO ($\rho = 4.8^\circ$ at 285nm) combined with tight focusing further restricts the crystal length to 5-7 mm and results in highly elliptical e-wave SH beam shape. Such a power limitation prevents from loading a dense MOT from a Zeeman-slowed thermal atomic beam [5].

To increase the interaction length and cancel the walkoff effect, an alternative to birefringent oxo-borate crystals may be to use nowadays available periodically-poled ferroelectric materials that employ quasi-phase-matching (QPM), i.e. periodic domain polarity reversal every micrometer-scale coherence length $l_{\text{coh}} = \pi/\Delta k$ [6,7,8]. Among them, pp-LiTaO₃ possesses the largest UV band gap ($\lambda_g = 280$ nm) but the broad UV absorption band (due to intrinsic lattice defects or transition metal ions impurities [9]) extending from the band edge to ~ 400 nm limits their use to single-pass interactions. With an absorption coefficient in the range 300-350 nm as high as $\alpha \leq 2$ cm⁻¹ (as

* Corresponding author

Email address: jjz@cnam.fr (J.-J. Zondy).

compared to $\alpha \leq 0.1 \text{ cm}^{-1}$ for BBO [10]), the absorbed UV radiation will cause severe thermal lensing effects and photo-refraction within any external enhancement resonator, as it was reported at an even longer blue wavelength (473 nm) for pp-KTP for instance [11], although thermal lensing was subsequently minimized by using looser cavity waists [12]. Furthermore, for short (micrometer-scale) deep-UV coherence lengths, the uniformity of grating periods $\Lambda = \lambda_\omega/2(n_{2\omega} - n_\omega)$ and of the 50% duty-cycle ratio required for first-order QPM is a challenging issue [13]. Using a second-order QPM at $\Lambda = 2.65 \mu\text{m}$ for the single-pass generation of $\lambda = 325 \text{ nm}$ in pp-LiTaO₃, Meyen *et al* measured a reduced effective nonlinear coefficient of only $d_{\text{eff}} = 2.6 \text{ pm/V}$ due to the combined effect of UV absorption and grating pitch imperfections [13].

Hence due to the lack of low-loss periodically poled materials for the UV range, generating watt-level cw light in the deep UV using birefringent material is a formidable task, except at specific wavelengths such as 266nm for which powerful (up to 15W cw) green frequency-doubled Nd:YVO₄ single-frequency lasers are readily available [14]. Among the few deep UV transmitting materials (KDP, ADP, LBO, CLBO, BBO) [10], BBO remains the best compromise owing to its larger UV bandgap ($\lambda_g = 280 \text{ nm}$), high UV damage threshold ($I_{\text{th}} \sim 1 \text{ GW/cm}^2$) and its larger nonlinearity ($d_{\text{eff}} \leq 2 \text{ pm/V}$, i.e. $\sim 3 \times$ that of LBO, $\sim 2.2 \times$ that of CLBO and $\sim 5 \times$ that of KDP). Although the recently introduced bismuth triborate material (BiB₃O₆ or BIBO [15]) with twice larger nonlinearity and lower walkoff than BBO cannot be used for the generation of deep UV below $\sim 350 \text{ nm}$, because of its limited useful transmission range for cw applications necessitating thick samples of the order of 1 cm. The advantage of using larger nonlinearity crystals in resonator-enhanced SHG stems from the lesser sensitivity of the parametric conversion yield to impedance-matching conditions, when the round-trip nonlinear loss ΓP_c (where Γ – see Eq. (1) – is the nonlinear efficiency in unit of W^{-1} and P_c is the circulating fundamental power) exceeds by far the linear passive fractional loss L_{RT} , a condition easily realized with periodically-poled crystal owing to their large d_{33} nonlinear coefficients [12]. Under the latter condition ($\Gamma P_c \gg L_{\text{RT}}$), the optimal input coupler transmissivity T_{opt} increases indeed ($T_{\text{opt}} \gg L_{\text{RT}}$), and the overall efficiency becomes insensitive to the lumped passive resonator loss. The drawback of BBO is however its ten-fold smaller effective nonlinear coefficient d_{eff} and the large walk-off angle ($\rho \geq 80 \text{ mrad}$) of the deep UV SH beam, limiting hence the focused-beam interaction length to a few millimeters. Furthermore, this huge walk-off combined with type-I strong focusing results in highly elliptical UV beam shape that needs to be spatially filtered for use in a 3D MOT, at the expense of detrimental power loss.

It is well known that walkoff compensation increases the coherence length of critical birefringence phase-matching. Producing powerful cw laser sources with good beam quality in the deep UV spectral range with BBO can be devised by taking profit of the single-pass efficiency enhancement of the mono-

lithic (optically-contacted) walkoff-compensation technique labelled as $2N$ -OCWOC structure [16]. $2N$ -OCWOC structures are periodic devices of length $L_c = 2Nl_c$, consisting of $2N$ ($N = 1, 2, \dots$ is the pairing number) crystal plates of thickness l_c rigidly stacked by optical adherence (and eventually diffusion-bonded, $2N$ -DBWOC) in the walk-off compensating configuration. Compared with the standard walkoff-compensation technique employing independently rotated multiple crystals (see, e.g., Refs. [17,18,19]), the compactness of monolithic $2N$ -OCWOC or $2N$ -DBWOC devices allows an improved crystal structure confinement within the near-field range of a tightly focused beam, eliminating the need for inter-plate facets anti-reflection (AR) coating (only the outer structure facets need eventually to be AR-coated). The detailed principle of operation of these structures has been thoroughly analyzed in Ref. [16], and their fabrication will be further outlined in Section 2. The principle of operation of $2N$ -OCWOC periodic structures is fundamentally different from the QPM technique, in the sense that each plate of the stack is birefringently phase-matched (hence the plate thickness can be arbitrarily chosen, but should approximately match the walkoff aperture length $l_a = \sqrt{\pi}w_0/\rho$ for an efficient walkoff compensation). Consequently $2N$ -OCWOC structures are conditioned to the pre-requisite occurrence of birefringence phase-matching, unlike the *à la carte* phase-matching tailoring capability of QPM structures. A second difference with QPM crystals is that the relative sign of the nonlinear coefficient d_{eff} from plate to plate must remain unchanged in order to avoid backconversion of the parametric process, whereas in QPM crystals this sign is reversed every coherence length l_{coh} so as to provide constructive interference along the periodic structure. This constraint on how to keep the same relative sign of d_{eff} in walkoff-compensating schemes is not trivial and has been previously extensively devised [17,18,19]. Another limitation of $2N$ -OCWOC structures stemming from the *frozen* relative orientation of the adhered plates is that they work efficiently only near normal-incidence phase-matching (PM) and require thus an accurate match of the cut angle θ_{cut} of all plates to the phase-matching angle θ_{PM} of the target fundamental wavelength. Hence extensive angular tuning is precluded contrary to bulk birefringent crystals, because at incidence angles exceeding the angular tuning bandwidth of each plate, one plate over two will not be phase-matched because of the crossed relative optic axis direction stemming from walkoff compensation [16]. Hence only temperature tuning at fixed normal incidence via the thermo-optic properties of the material is possible for moderate wavelength tuning. This angular tunability restriction renders the fabrication of $2N$ -OCWOC devices extremely challenging for large birefringence materials as BBO because of its narrow angular acceptance bandwidth ($\Delta\theta \cdot L \leq 0.015^\circ \cdot \text{cm}$) as compared with KTP. Due to the unavoidable angle cut uncertainty (typically $\Delta\theta_{\text{cut}} \simeq \pm 0.2^\circ$ from X-ray orientation), and given the $\Delta\theta_{\text{PM}} \sim \pm 0.5^\circ$ inaccuracy of the best Sellmeier dispersion relations, the design of BBO periodic structures requires hence preliminary stringent tests aimed at determining the PM angle to a precision equivalent to the acceptance angle $\Delta\theta$ of each plate. Finally, small relative

crystallographic orientation mismatches of the stacked plates were found to be responsible of enhancement reduction accompanied by bandwidth broadening [16].

$2N$ -OCWOC structures have been until now successfully implemented in type-II critically phase-matched SHG of 1064 nm laser with a KTiOPO_4 (KTP) 10-plate structure, leading to a record single-pass enhancement factor of up to $22\times$ compared with a bulk KTP for SHG at 1064 nm [20]. A 4-plate KTP structure ($N = 2$) was also used for enhanced frequency-doubling of $2.53\ \mu\text{m}$ color center laser [21], and a 2-OCWOC RbTiOAsO_4 (RTA) tandem has led to a $3.7\times$ enhancement for the SHG of a $1.32\ \mu\text{m}$ Nd:YAG laser [22]. In this latter experiment, walkoff-compensation also allowed to perform cascaded third-harmonic generation into the blue by sum-frequency generation of the residual spatially recombined $1.32\ \mu\text{m}$ o and e waves with the generated red o-wave exiting the tandem structure in the sum-mixing crystal. Although for type-I coupling, only a moderate enhancement as compared with type-II is predicted [16] (in type-I coupling, the oo or ee polarization wave radiates along the whole crystal length while in type-II it ceases to radiate as soon as the two o and e components walk off), the advantage of a UV beam shape re-circularization thanks to walkoff compensation cannot be neglected [16].

In this work, we investigate for the first time the fabrication of deep UV monolithic walk-off compensating structures with type-I (ooe) birefringence phase-matched BBO. Due to the large birefringence of BBO ($\Delta n \sim 0.12$ and related vanishing angular acceptance bandwidth), we have chosen as a starting step to characterize first a 2-OCWOC device with length $L_c = 8\ \text{mm}$ ($N = 1$, i.e. 2 contacted plates with $l_c = 4\ \text{mm}$) prior to the design of a more complex structure employing up to 10 ($N = 5$) optically-contacted plates. The 2-OCWOC tandem actually constitutes the basic unit cell of $2N$ -OCWOC periodic structures (section 2). This preliminary step allows further to test the feasibility and quality of optical adherence with BBO, and to highlight the main important parameters for the design of a more complex tandem structure. As compared with type-I non-monolithic BBO walkoff-compensating devices, for which the relative orientation of the plates can be independently controlled so as to broaden the overall phase-matching bandwidth [18,19], we shall confirm the prediction of the $2N$ -OCWOC cw theory [16] as to the limited and finite acceptance bandwidth characterizing a frozen-orientation OCWOC tandem (section 3). We also demonstrate that at the optimal design wavelength corresponding to normal-incidence phase-matching, a nearly two-fold enhancement (with respect to a bulk BBO sample of identical length) of the SH conversion efficiency of the 2-OCWOC tandem is obtained, as predicted by the theory (section 5). Additionally, we provide an accurate measurement of the type-I BBO effective nonlinearity for UV generation, in agreement with recent measurements. We finally conclude from these preliminary investigations on the relevant procedures to design even more efficient complex structures with an

arbitrary number of plates, so as to circumvent the stringent accuracy limitations imposed by the large medium birefringence (section 6). The chosen target UV wavelength ($\lambda = 285.217$ nm) corresponds to the $^1S_0 - ^1P_1$ Doppler cooling transition of Mg, but could be any wavelength above the $\lambda_g \sim 180$ nm UV transmission cut-off of BBO. The walkoff angle experienced by the extraordinary SH wave is $\rho = 4.8^\circ = 84$ mrad at 285 nm, yielding a short cylindrical beam aperture length of $l_a = \sqrt{\pi}w_0/\rho = 21w_0$. For a typical fundamental waist $w_0 \sim 50$ μ m, the bulk aperture length is about $l_a = 1$ mm. Let us note that in focused beam geometry and using a bulk BBO, the typical maximum length that optimizes the conversion efficiency for a waist in the range $20 - 30$ μ m is about $L_c = 5 - 7$ mm. Beyond this length, the dephasing of the walking-off SH e-wave with respect to the fundamental o-wave polarization results in extremely sharp ellipticity of the SH beam. The use of a $2N$ -OCWOC structure with $N > 1$ would allow to increase this interaction length while minimizing the UV beam ellipticity and releasing the vanishing-bandwidth constraint.

2 2-OCWOC tandem principle and fabrication

If two identically cut crystals are cascaded such that their optical axes (c) are crossed with respect to a plane perpendicular to the light propagation z-axis, the internal Poynting vector \mathbf{S}_e of the walking-off wave in the second crystal is reversed (symmetry with respect to z) with respect to its direction in the first crystal. Hence walkoff compensation in birefringent media takes profit of the principle of the inverse return of light upon a mirror-like folding process (Fig. 1). From the point of view of harmonic generation, the two cascaded crystals are equivalent to a double-passed single crystal using a back-reflecting mirror (or a multi-pass SHG in a semi-monolithic concave-plano resonator [23]), provided that the phase-shift of the waves due to mirror reflection does not reverse the sign of the nonlinear coefficient.

The design of a unit-cell 2-OCWOC tandem may start from an oriented bulk sample of length L_c ($\theta \equiv \theta_{PM}$ in Fig. 1 being the PM angle between the optic axis and the normal to the facets) that is sliced into 2 plates of identical length $l_c = L_c/2$. The second plate is then rotated by 180° along an axis either perpendicular or parallel to the propagation axis, so as to reverse the relative sign of walkoff ($+\rho \rightarrow -\rho$) from one plate to the other (Fig.1). The choice of the rotation axis, which depends on the polarization configuration of the interacting waves, is dictated by the conservation of the relative sign of the nonlinear coefficient ($+d_{\text{eff}} \rightarrow +d_{\text{eff}}$) as extensively discussed in Refs. [17,18], in order to avoid back-conversion of the SH wave. In the case of type-I(ooe) coupling, the rotation axis is perpendicular to the propagation axis. The length matching accuracy of the plates is not as stringent as in QPM structures, because the plane-wave coherence length of birefringence phase-matching is in

principle infinite. For a pairing number $N > 1$, the e-wave Poynting vector is then "birefringence-guided" throughout the structure and confined along the o-wave propagation axis, which is equivalent - to first order approximation - to an effective reduction of the walkoff angle ($\rho_{\text{eff}} \sim \rho/2N$) for the OCWOC structure.

The 2-OCWOC plates of length $l_c = 4$ mm (aperture 4×4 mm²) used here were diced from a single bulk BBO element oriented at $\theta = 43.2^\circ$ ($\varphi = 30^\circ$), with an accuracy of $\sim 0.1 - 0.2^\circ$. The chosen plate length $l_c = 4$ mm corresponds to one aperture length l_a for a waist value $w_0 = 188$ μm . Let us note that the predicted BBO phase-matching angle determined from various Sellmeier equations [10] may differ by more than $\pm 1^\circ$ from the chosen orientation. Due to the extremely small acceptance bandwidth of BBO, it is expected that normal incidence phase-matching would not exactly match the target wavelength (hence a tunable laser such as the dye laser used for pumping is necessary to characterize the 2-OCWOC structure). Care was taken so that the sawing process and subsequent fine plate polishing required for optical adherence did not affect the relative orientation of the resulting plates, which would be detrimental to the conversion efficiency due to the vanishing acceptance angle bandwidth of the phase-matching. The contacted plate facets have the following specifications: flatness not less than $\lambda/8$, parallelism not larger than 20 arc seconds, surface finish better than 10/5 scratch/dig. After careful hand-polishing, the two plates were then brought into optical adherence to form the 2-OCWOC tandem. The two outer structure facets were left uncoated for this preliminary testing. Let us note that despite all these precautions, the sawing and polishing processes may introduce residual slight relative orientation cut from one plate to the other, the effect of which has been found to broaden the phase-matching bandwidth at the expense of the enhancement factor brought about by the walkoff compensation effect [16,20]. Such effects are minimal when the relative orientation mismatch angle is small enough compared to the acceptance angle of a single plate ($\Delta\theta \sim 0.04^\circ$).

An available uncoated BBO witness bulk sample with identical length $L_c = 8$ mm as the 2-OCWOC tandem was used for conversion efficiency comparison purpose. For this bulk sample, the orientation accuracy did not matter since slight angular tuning allows to phase-match any wavelength around the targeted one. The quality of the optical contact of the 2-OCWOC tandem was checked by comparing its transmission spectrum with that of the bulk witness sample. No significant difference of transmittance was noted. We have used further the focused yellow laser, which allowed to scan the focused spot over the 2-OCWOC aperture, for direct transmission comparison. Both methods gave identical transmission factor for the two samples, indicating that good optical contact was obtained over more than 80% of the total aperture. The absence of spurious Fresnel reflection other than the specular reflection from the input facet was another indication of the quality of the adhered surfaces.

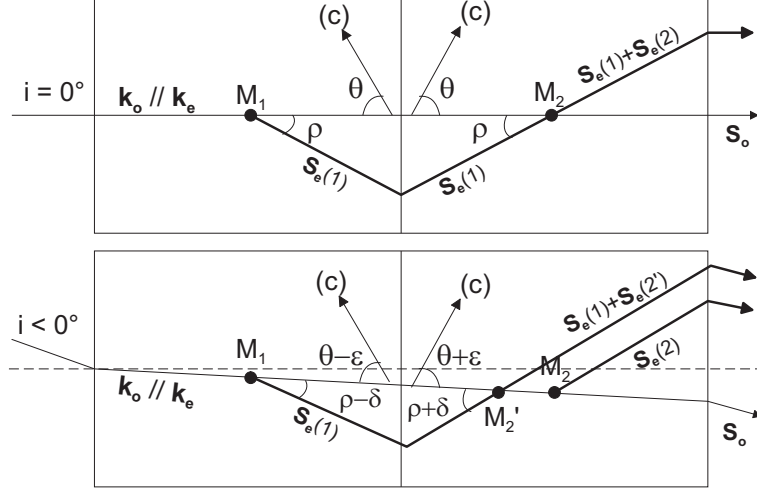


Fig. 1. Schematics of a 2-OCWOC tandem structure for type-I(ooe) phase-matching, showing the crossed optic axes (c). Note that by symmetry about the normal incidence axis, in the lower panel an incoming $i > 0$ ray will produce at the output SH Poynting vectors emerging at a symmetric direction (upward) from the sketched arrows. See text for further explanations.

As pointed out in the introductory section, the limited angular tunability imposed by the frozen relative orientation of the plates is explained in Fig.1 which sketches the case of a fundamental o-wavevector $\mathbf{k}_o(\omega)$ (out of the bundle of wavevectors of the Gaussian beam) impinging either at $i = 0^\circ$ (upper frame) or at an oblique incidence $i \neq 0$ (lower frame), in the ideal case that no relative $\theta = \theta_{\text{PM}}$ orientation mismatch exists between the 2 plates. The e-wave Poynting vectors \mathbf{S}_e of the SH generated by two symmetrically located dipoles belonging to either the first plate (M_1) or the second (M_2) are shown. For $i = 0^\circ$ both SH rays overlap and interfere at M_2 with a phaseshift dictated by the collinear PM condition $\Delta k = \mathbf{k}_e(2\omega, \theta) - 2\mathbf{k}_o(\omega) = 0$. Away from $i \simeq 0$, due to the periodic flip of the optic axis (c) direction from plate to plate and to the fact that wavevectors \mathbf{k}_i ($i = o, e$) are not refracted at the boundaries (no index discontinuities), a phase-mismatch grating $\pm\delta k = \pm\varepsilon\partial\Delta k/\partial\theta$ arises under oblique incidence due to the $\theta \pm \varepsilon$ angles that the \mathbf{k}_i 's make with the optic axes [16]. However as long as ε is kept small compared with the FWHM acceptance bandwidth $\Delta\theta \simeq 0.88\lambda_\omega/(\rho l_c n_{2\omega, e})$ of the PM, enhancement may still arise whereas when $\varepsilon \gg \Delta\theta$, only one plate would contribute to the SH signal. The $\theta \pm \varepsilon$ apparent orientations of the plates further result in slightly different walkoff angles $\rho \mp \delta$ upon crossing the boundary, since walkoff angle expresses as $\rho(\theta) = \frac{1}{n_e(\theta)}\partial n_e/\partial\theta$. Since $\varepsilon \simeq i/n_{\omega, o}$, the difference is of second-order, $\delta = \varepsilon[\partial\rho/\partial\theta]_{\theta_{\text{PM}}}$. It follows from Fig. 1 (bottom frame) that $\mathbf{S}_e(1)$ crosses the polarization wave ahead of M_2 with a different dephasing with the SH radiated by M_2' due to the phase-mismatch grating. It is then clear that the efficiency enhancement experienced by normal incidence PM should be larger. Under loose plane-wave focusing and for a small acceptance bandwidth, two separate SH intensity peaks should appear in angular tuning mode if the 2-

OCWOC cut angle does not exactly match the target wavelength (section 5).

3 Theoretical background

The SH conversion efficiency $\Gamma_N = P_{2\omega}/P_\omega^2$ (in W^{-1} unit) of an *ideal* $2N$ -OCWOC structure (i.e. free of orientation mismatches), characterized by a walk-off parameter $B = \frac{1}{2}\rho\sqrt{k_\omega L_c}$ ($k_\omega = 2\pi n_\omega/\lambda$ is the fundamental wavevector) [24], and for a beam focusing parameter $L = L_c/z_R$ ($z_R = \frac{1}{2}k_\omega w_0^2$), can be cast as [16]

$$\Gamma_N(B, L) = KL_c k_\omega h_N(\sigma_1, \sigma_2), \quad (1)$$

where $K = (2\omega^2/\pi\epsilon_0 c^3)(d_{\text{eff}}^2/n_\omega^2 n_{2\omega})$ is the SHG constant factor and $\sigma_{1,2} = \Delta k_{1,2} z_R$ are the reduced wavevector mismatches of the two twinned plates forming the unit cell of the periodic structure. For an angular tuning, $\sigma_2 = -\sigma_1$ (due to the $\pm\Delta k(\theta)$ wavevector grating) whereas at fixed normal incidence ($i = 0^\circ$, $\theta = \theta_{\text{PM}}$) and under either wavelength or temperature tuning, one has $\sigma_2 = \sigma_1 = \sigma(\lambda, T)$. For the simplest case of $N = 1$, and considering normal incidence tuning ($\sigma_1 = \sigma_2 = \sigma$), the focusing (aperture) function h_1 in Eq. (1) simplifies as [22]

$$h_1(\sigma) = \frac{1}{L\sqrt{\pi}} \int_{-\infty}^{+\infty} du e^{-4u^2} \left| \int_0^{L/2} d\tau \left[\frac{e^{-i(\sigma-4\beta u)\tau}}{1+i\tau} + \frac{e^{+i(\sigma+4\beta u)\tau}}{1-i\tau} \right] \right|^2. \quad (2)$$

The parameter $\beta = \rho/\delta_0$ is the walkoff angle normalized to the fundamental Gaussian beam internal divergence $\delta_0 = \lambda/(\pi n_\omega w_0)$. The integration variable u is the SH far-field angular transverse coordinate in the walk-off plane (x -plane, the y -plane being the walkoff-free transverse plane), normalized to δ_0 [16,25]. The kernel $\exp(-4u^2)|F(u)|^2$ of the u -integral in Eq. (2) gives hence the y -integrated *far-field* intensity distribution of the SH wave in the walkoff plane, which departs from the y -plane Gaussian one ($\exp(-4v^2)$). The quantity inside brackets in Eq. (2) accounts for the interference effects leading to SH enhancement as the normalized phase-mismatch σ is tuned. Eq. (2) has to be compared with the focusing function of the witness bulk non walkoff-compensated crystal ($N = 0$) [16,25],

$$h_0(\sigma) = \frac{1}{L\sqrt{\pi}} \int_{-\infty}^{+\infty} du e^{-4u^2} \left| \int_{-L/2}^{+L/2} d\tau \frac{e^{-i(\sigma+4\beta u)\tau}}{1+i\tau} \right|^2. \quad (3)$$

The walk-off compensation effect manifests in the increased value of the focusing function h_N and in the re-circularization of the transverse intensity profile as the number N of twinned cells is increased. Actually for $N \rightarrow \infty$ (keeping the structure length constant) and at the optimal focusing parameter L_{opt} ,

the function h_N asymptotically approaches $h_0 \simeq 1.068$ which is the optimal value of the focusing function for a non-critically phase-matched bulk crystal ($B = 0$) [16]. However the tuning bandwidth does not diverge but remains finite, as a consequence of the critical phase-matching.

The walkoff parameter for the $L_c = 8$ mm long BBO tandem or bulk sample is as large as $B = 16$ for the generation of $\lambda_{SH} = 285.2$ nm. Optimization of the focusing functions (2)-(3) over the residual phase-mismatch parameter σ , for a waist location at the middle of either sample, yields a smooth optimum in the range $w_0^{\text{opt}} = 18 - 22\mu\text{m}$ ($L \sim 2$) for both, with $\sigma_{\text{opt}}(\text{bulk}) = -1.0$ while $\sigma_{\text{opt}}(2\text{-OCWOC}) = -0.91$. Non-zero value for σ_{opt} under strong focusing traduces the usual trade-off between diffraction and walkoff that introduce additional transverse wavevector components. For comparison sake with the experimental waist that was closest to the mathematical optimum ($w_0 = 25$ mm, focusing parameter $L = 1.38$), in Fig.2 we have plotted with solid line the wavelength or temperature tuning curve (proportional to $h_1(\sigma)$) of the 2-OCWOC tandem as function of the overall phase-mismatch $\Phi = \sigma L/2 = \Delta k(\lambda, T)L_c/2$ (in radian unit).

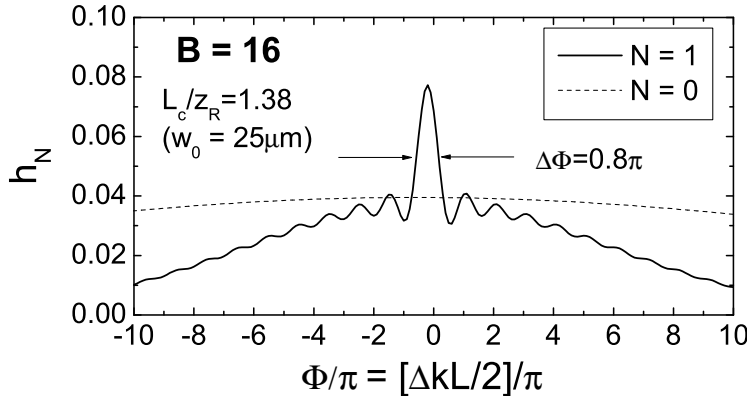


Fig. 2. Theoretical wavelength tuning curve of the ideal BBO 2-OCWOC tandem ($N = 1$) in comparison with that of a non walk-off compensated bulk sample ($N = 0$). The optimal values of the focusing functions and conversion efficiencies are: $h_0^{\text{opt}} = 0.03933$, $\Gamma_0^{\text{opt}} = 1.054 \times 10^{-4} \text{ W}^{-4}$ and $h_1^{\text{opt}} = 0.07722$, $\Gamma_1^{\text{opt}} = 1.80 \times 10^{-4} \text{ W}^{-4}$. The Γ_N values assume $d_{\text{eff}} = 1.7 \text{ pm/V}$ ($K = 1.8039 \times 10^{-8} \text{ W}^{-1}$).

The curve displays a sharp enhancement peak due to the constructive interference contribution from both plates, lying over a broad pedestal whose maximum intensity is that of the tuning curve of a non walk-off compensated bulk witness sample of identical length L_c (dashed curve, $N = 0$). While the plane-wave $\text{sinc}^2(\Phi)$ bandwidth function should yield a narrow FWHM bandwidth of $\Delta\Phi \simeq \pi$ comparable to the peak width, the broadening of the pedestal - corresponding to the non interfering contribution from each plate - is due to the combined effect of strong focusing and large walkoff angle. The predicted type-I enhancement efficiency $h_1/h_0 = 0.0772/0.0393 = 1.96$

is moderate because the plate length is still several times the aperture length $l_a \simeq 0.53$ mm. Because the peak width scales like the plane-wave bandwidth, using the dispersion properties of BBO one can predict a FWHM wavelength tuning bandwidth within the peak of $\Delta\lambda \sim 0.15$ nm. Such a frequency range ($2 \times \Delta\nu \simeq 276$ GHz in the UV range) is usually sufficient to span the hyperfine structure or isotope shift of an atomic transition line.

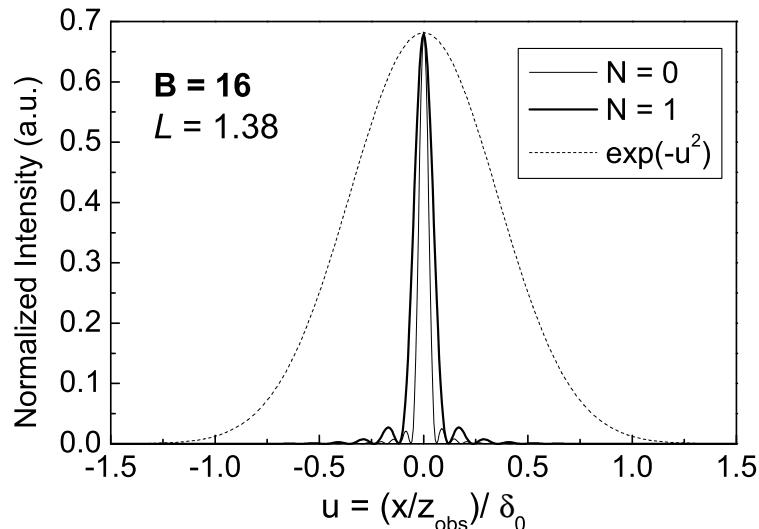


Fig. 3. Far-field normalized SH beam transverse profile at the optimal Φ_{opt} values of Fig.2. The dashed Gaussian pattern depicts the walkoff-free pattern in the vertical direction.

In Fig.3, the far-field normalized u -transverse intensity patterns in the plane perpendicular to the walkoff plane (as given by the kernel of Eqs. (2)-(3)) are plotted at $\sigma = \sigma_{\text{opt}}$. Note that free-space propagation to a distance $z_{\text{obs}} \gg L_c$ inverts the ellipticity of the UV beam (the far-field pattern is the Fourier transform of the near-field one). As compared with the Gaussian y -profile (dashed line), the x -profiles are highly compressed, displaying some tiny oscillatory diffraction pattern at their wings. The ellipticity of the 2-OCWOC beam profile is seen to be slightly reduced as compared with that of the bulk crystal. Clearly, for $L_c = 8$ mm the number of twinned plates must be increased for a substantial improvement in beam shape quality (see section 6).

4 Experimental setup and measurement procedures

The experimental setup is sketched in Fig.4. The frequency-stabilized, single-longitudinal mode rhodamine 6G dye laser is widely tunable around the target fundamental wavelength of $\lambda = 2\lambda_{\text{UV}} = 570.434$ nm, by tuning the intra-cavity Lyot filter. Typically, the laser delivers a power of 1.7 W with a linewidth of 1.3 MHz and nearly perfect Gaussian beam shape. The wavelength is measured by

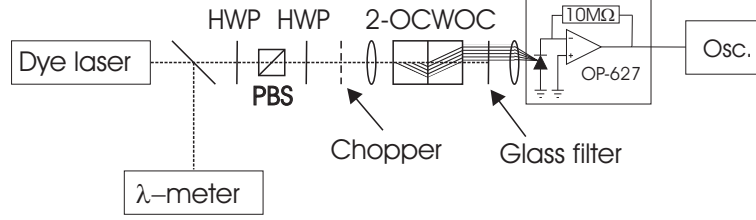


Fig. 4. Schematics of the experimental setup. HWP: half-wave plate, PBS: polarizing beam splitter cube.

a wavemeter with an accuracy of ± 0.001 nm for wavelength measurements. The yellow beam power can be attenuated by a half-wave plate followed by a polarisation beam splitter. A second half-wave plate permits the optimisation of the final "ordinary" (vertical) polarisation for the fundamental wave. For convenient UV power detection on an oscilloscope, the laser beam is chopped at about 200 Hz and focused into the BBO samples (2-OCWOC tandem or bulk witness BBO) with a set of lenses (focal lengths $f = 80 - 500$ mm). The crystal is mounted on a rotation stage with a resolution of 0.016 degree for angular bandwidth measurements. The rotation stage is attached to a xyz-positioner for optimization of the focusing conditions. Care was taken not to clamp the 2-OCWOC tandem in order to avoid mechanical stress that may disrupt the optical contact. A 2 mm thick Schott glass filter (UG11) located behind the crystal transmits 64 % of the UV light and completely blocks the fundamental power ($T < 10^{-10}$). To avoid thermal damage of the absorptive glass filter due to the tight focusing, the fundamental power has to be limited to about 400 mW. The UV light is focused by a $f = 50$ mm collecting fused-silica lens on the small area (1.1 mm^2) Si photodiode with a calibrated responsivity of $r=0.113$ A/W at 285.2 nm. The photocurrent is converted into voltage with a transimpedance amplifier based on a low noise, low offset voltage and large gain-bandwidth product operational amplifier chip (OPA627) with a 10 M Ω load resistor. The voltage-to-power conversion is 1.13 mV/nW. Since the voltage noise, given by the oscilloscope trace thickness, was about 5 mV it was possible to detect down to a few nW UV of light. All SH powers $P_{2\omega}$ reported hereafter correspond to a fixed fundamental power of $P_{\omega} = 400\text{mW}$, so that every displayed conversion efficiency curve gives the net absolute UV generated power for a constant reference power ($P_{\omega} = 0.4$ W), after correction for the transmissivity losses of the uncoated crystal facets ($n_{\omega} = n_{2\omega} = 1.67$ at $\lambda = 570.4$ nm) and glass filter. The UV generated power did not vary more than 10% when the laser focus is scanned over 80% of the samples aperture, the fluctuations being due to some sparse scattering points in the BBO samples. Let us recall that the fundamental transmission loss of

the bulk and 2-OCWOC samples were found identical.

5 Experimental results

In a first step the wavelength tuning curve of the 2-OCWOC structure (set at normal incidence) was characterized in order to determine its actual design wavelength λ_0 .

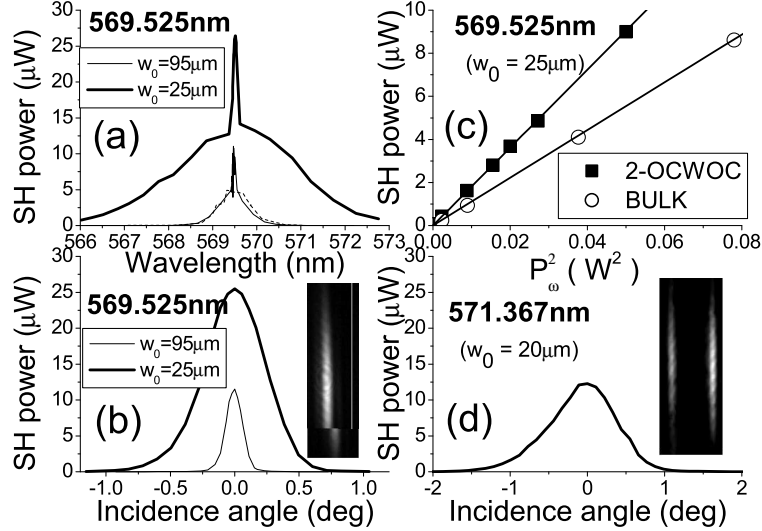


Fig. 5. (a): Wavelength tuning curves of the 2-OCWOC tandem for two focusing parameters (loose and near optimal). The tandem is set at normal incidence. The predicted enhancement peak in the wavelength tuning curve occurs at $\lambda_0 = 569.525 \text{ nm}$. (b): Angular tuning curve at $\lambda_0 = 569.525 \text{ nm}$, again for the loose and strong focusing parameters. (c): Optimal conversion efficiency of the tandem at λ_0 compared with that of the bulk sample, showing an efficiency enhancement of 1.65. (d): Angular tuning curve at the target wavelength, i.e., at $\Delta\lambda_0 \sim +1.9 \text{ nm}$ above λ_0 . The comparison of (b) and (d) highlights the critical issue of matching the cut angle to the target wavelength.

Fig.5(a) shows the results for a loose ($w_0 = 95 \mu\text{m}$) and for a near optimal strong focusing conditions ($w_0 = 25 \mu\text{m}$). Indeed, a sharp enhancement peak lying over a broad pedestal spanning over $\sim 6 \text{ nm}$ for the strongest focusing – as predicted in Fig.2 in terms of Φ variable – is apparent but at $\Delta\lambda_0 \simeq -1 \text{ nm}$ ($\lambda_0 = 569.525 \text{ nm}$) from our target wavelength ($\lambda = 570.434 \text{ nm}$). This unfortunate discrepancy originates from the insufficient accuracy in matching the BBO cut angle (θ_{cut}) to the actual PM angle (θ_{PM}), as previously discussed, given the unavoidable inaccuracy of dispersion relations and crystal orientation. The experimental peak width $\Delta\lambda_{\text{FWHM}} \simeq 0.2 \text{ nm}$ is in agreement with the theoretical peak width expressed in Φ unit in Fig.2, and compares also surprisingly well with the plane-wave spectral bandwidth of the bulk equivalent crystal, $\Delta\lambda_{\text{PW}} = 0.15 \text{ nm}$. The intensity and width of the broad pedestal match approximately those of the wavelength tuning curve of the bulk wit-

ness sample (not shown for clarity sake). The pedestal broadening effect for strong focusing can be noticed, as in the angular tuning curves taken at a fixed $\lambda = \lambda_0$ [Fig.5(b)].

When the laser wavelength was tuned to $\sim \pm 1\text{nm}$ away from λ_0 , the enhancement in conversion efficiency vanishes despite additional angular tuning [Fig.5(d)], and the maximum UV power is then identical to or slightly lower than that obtained with the bulk sample. This demonstrates that away from λ_0 the contribution of both plates are independent (no interference effect). Actually, the UV profiles captured at $z_{\text{obs}} = 20\text{ cm}$ by a CCD camera for $\lambda = \lambda_0$ (inset of 5(b)) and $\lambda = \lambda_0 - \Delta\lambda_0\text{ nm}$ (inset of 5(d)) show that the transverse profile is a single elliptical spot in the first case, whereas two adjacent ellipses appear for the second case as a proof that the UV Poynting vectors do not overlap for this slightly oblique incidence PM. In the angular tuning curve of Fig.5(d), the strong diffraction hinders the observation of two separate maxima, but the non normal incidence effect described in Fig.(1) manifests in the far-field profile of the SH wave. Let us mention that contrary to the 2-OCWOC tandem, the tuning curve shapes (angular or wavelength) and UV intensity of the witness bulk crystal were wavelength insensitive.

In Fig.5(c), the SH power $P_{2\omega}$ at the optimal $\lambda = \lambda_0$ and focusing is plotted against P_{ω}^2 , displaying an efficiency enhancement factor of $\Gamma_{N=1}/\Gamma_{N=0} \simeq 1.65$ respective to the non walk-off compensated crystal. The measured enhancement value is close to the one predicted in Fig.(2), i.e. $h_1/h_0 = 1.96$. This enhancement due to walkoff-compensation is equivalent to an enhancement of the bulk effective nonlinearity, $d_{\text{eff}}(N=1)/d_{\text{eff}}(N=0)$, by a factor $\sqrt{1.65} = 1.28$. Because our absolute power measurements are accurate to $\pm 5\%$, we were able to check the nonlinear coefficient value of BBO in the UV range. From the measured absolute UV conversion efficiency derived from the slope of the bulk conversion efficiency in Fig.(5(c)), $\Gamma_{N=0} = 1.105 \times 10^{-4}\text{ W}^{-1}$ and the corresponding value of the focusing function $h_0 \simeq 0.03933$, using formula (1) with $K = 6.2419 \times 10^{+15} d_{\text{eff}}^2$ (in SI unit) one can derive a value of the effective nonlinear coefficient of BBO at 285 nm, $d_{\text{eff}}(285\text{ nm}) = 1.75\text{ pm/V}$. This value is very close to the value assumed in the caption of Fig.2, and also identical to the value reported for the SHG at 266nm in Ref. [14]. The related uncertainty should not exceed $\pm 10\%$ despite the fact that we have neglected the UV absorption of BBO ($\alpha_{2\omega} \sim 0.05\text{ cm}^{-1}$ [10,26,27]). Since for type-I(ooe), $d_{\text{eff}}(\theta, \varphi) = d_{31} \sin(\theta + \rho) - d_{22} \cos(\theta + \rho) \sin 3\varphi$ and using the much smaller value of $d_{31} = 0.04\text{ pm/V}$ [28] ($|d_{31}| \ll |d_{22}|$) with opposite signs for the two nonlinear tensor components), one can derive a new value $d_{22} = 2.57\text{ pm/V}$ valid for deep UV generation. This measurement confirms the value measured from Maker fringes at 1064nm by Shoji et al [28], who found $d_{22} = 2.6\text{ pm/V}$.

Having determined the design wavelength $\lambda_0 = 569.525(\pm 0.1)\text{ nm}$, and in order to get a further insight in the actual absolute and relative orientation

of both tandem plates, several angular tuning curves of the 2-OCWOC device were recorded at various wavelengths located around λ_0 , under a loose (quasi plane-wave) focusing condition allowing to screen off the broadening effect of strong diffraction. According to the simple ray picture of Fig.1 describing the behavior of the 2-OCWOC tandem under slightly oblique incidence phase-matching (hence away from λ_0), shining the tandem under cylindrical plane-wave condition (i.e. when beam divergence $\delta_0 = \lambda/\pi n_\omega w_0$ is small compared to the plate PM acceptance angle $\Delta\theta$) should result in the appearance of two PM peaks in the angular tuning behavior. The measurement of their angular position respective to normal incidence provides an accurate knowledge on the absolute cut angles of both plates, and also provides a mean to better match the design wavelength to the target wavelength, as we shall see further.

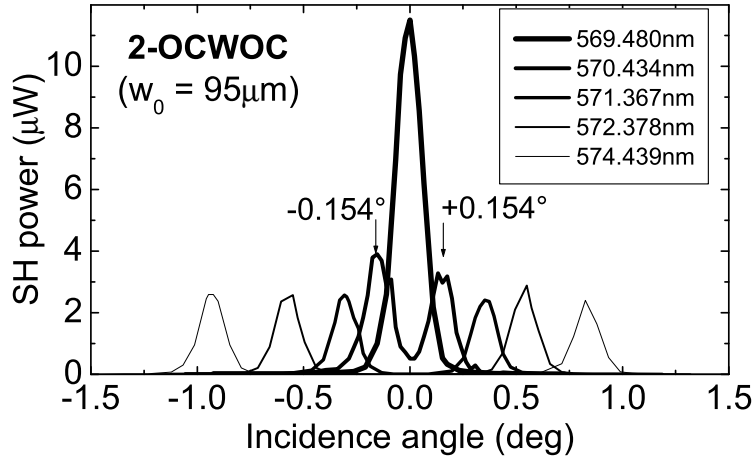


Fig. 6. Loose focusing ($L = 0.096$) angular tuning curves of the 2-OCWOC tandem at various pump wavelengths around the (normal incidence) design wavelength $\lambda_0 = 569.525$ nm.

Fig.6 displays the angular tuning patterns for several pump wavelengths around λ_0 . Away from λ_0 , the curves display indeed a well separate dual-peak feature, evidencing that the contributions from the 2 plates do not interfere due to the much reduced acceptance angle and to the non strictly normal incidence phase-matching. Under strong focusing, the broadening effect due to diffraction and walkoff washes out the 2-peak features as can be seen for the $\lambda = 571.367$ nm angular tuning curve at $w_0 = 20 \mu\text{m}$ (Fig.5(d)). The non-interfering feature is then evidenced by the appearance of two elliptical lobes in the far-field transverse pattern.

As the wavelength approaches λ_0 , the two peaks tend to merge into a single enhanced peak centered at $i = 0^\circ$, the amplitude of which is $4\times$ greater. Note that the corresponding wavelength on the plot ($\lambda = 569.480$ nm) does not exactly match λ_0 , even though it lies within the $\Delta\lambda_{\text{FWHM}} = 0.2$ nm enhancement bandwidth. The symmetric angular locations of the two peaks – with respect to normal incidence – in each of the curves is an indication that no relative ori-

entation mismatch between the two plates (that may originate from the optical contacting procedure) was introduced during the fabrication of the tandem. The $\delta\theta_{\text{cut}} = \pm 0.154^\circ/n_\omega \simeq \pm 0.09^\circ$ deviation measured on the $\lambda = 570.434\text{nm}$ curve in Fig. 6 allows to correct for the required BBO angle cut in the future design of a more efficient 8-OCWOC structure ($N = 4$). Such a small value – within the technical fabrication inaccuracy – highlights the difficulties in the design of $2N$ -OCWOC out of BBO. The sign (\pm) of the angle correction to be performed to the present value of θ_{cut} can be ascertained from the known linear dispersion of $\theta_{\text{PM}}(\lambda)$ in BBO. Since $d\theta_{\text{PM}}/d\lambda < 0$, the ($-$) sign applies to shift the design wavelength from $\lambda_0 = 569.525\text{ nm}$ to $\lambda = 570.434\text{ nm}$. This would imply to de-assemble the tandem and to wedge-polish both plates and check the wedge correction angle by use of optical or interferometric techniques prior to re-contacting them again.

Another alternative to match the target wavelength to the design wavelength is to set the tandem at $i = 0^\circ$ and employ temperature tuning to move the room temperature design wavelength to the target wavelength located by less than 1nm above. Such a temperature matching was recently used to demonstrate solitonic beam self-trapping in a 10-OCWOC KTP structure type-II phase-matched for the SHG of a pulsed 1064nm laser [30]. BBO has rather small birefringe in its ordinary and extraordinary thermo-optic coefficients [29]. The evaluation of the thermo-optic dispersion of PM angles at 570.5 nm SHG yields $d\theta_{\text{PM}}/dT \simeq +0.001^\circ/\text{K}$. In order to shift the PM angle by an amount $\pm 0.1^\circ$, one needs hence to heat or to cool the sample by $\Delta T \sim 100^\circ\text{C}$. Because in our case, negative $\Delta\theta_{\text{PM}} < 0$ correction is required, one has then to cool down the tandem to a cryogenic temperature, which is ruled out by technical constraints. If the correction sign to angle cut were positive, instead of being negative, a more convenient heating up to $T \sim 90^\circ\text{C}$ would have been possible. However, the anisotropic thermal expansion behavior of BBO (which has opposite signs of expansion in the directions parallel and perpendicular to the optic axis) must be taken into account to avoid disrupting the optical contact during the heating ramp phase. We plan to investigate in the future this thermal behavior of optical adherence in BBO $2N$ -OCWOC structures. To rule out the eventuality of contact breaks, the use of more rigid thermally diffusion-bonded structures ($2N$ -DBWOC) can be envisaged as with KTP [31].

6 Considerations for the design of an 8-OCWOC BBO structure

The above experimental analysis of the spectral and angular behaviors of the 2-OCWOC tandem highlights the extreme difficulties related to the optimal design of $2N$ -OCWOC structures out of the highly birefringent BBO, but also provides useful informations on the design criteria for a successful monolithic walkoff-compensating structure for the deep UV. A preliminary step is to

match the θ_{cut} angle as accurately as possible with the target wavelength $\theta_{\text{PM}}(\lambda_0)$, by using a preliminary bulk test sample. The accuracy of this match must be of the order of the phase-matching acceptance angle of each plate ($\Delta\theta \sim 0.04^\circ$ for $l_c = 4\text{mm}$).

Decreasing l_c down to 1mm will relax this matching tolerance to $\Delta\theta \sim 0.15^\circ$, a value close to the X-ray diffractometer uncertainty. From the present experiment, the orientation error sign should be preferably negative in order to use heat tuning for correction. In our case, keeping the structure length constant, the next step is then to increase the pairing number to, e.g. $N = 4$ ($l_c = 1\text{mm}$) or $N = 5$ ($l_c = 0.8\text{mm}$), since walk-off is far from being totally compensated with $N = 1$. The optimal plate length should correspond to the aperture length $l_a = \sqrt{\pi}w_0/\rho$ which, for $w_0 = 25\mu\text{m}$, is 0.5mm. The limiting factor for the pairing number N will be related to the technical handling and polishing of very thin plates. Note however that the overall acceptance bandwidth of the structure will not be broadened to that of a single plate as in non-monolithic walkoff-compensated devices [19] for which the rotational adjustment of each individual plate is allowed for phase compensation. In monolithic $2N$ -OCWOC devices, the overall bandwidth will depend on the *frozen* relative orientation mismatches among the plates, as pointed out in Ref. [16]. From the theory given in Ref. [16], the acceptance bandwidth cannot diverge as $N \rightarrow \infty$, but remains finite and equal to twice the acceptance bandwidth of the equivalent bulk sample.

For an *ideal* structure (no relative orientation mismatch), the perfectly periodic wavevector grating $\pm\Delta k$ leads actually to a nonlinear birefringent filter response of the structure.

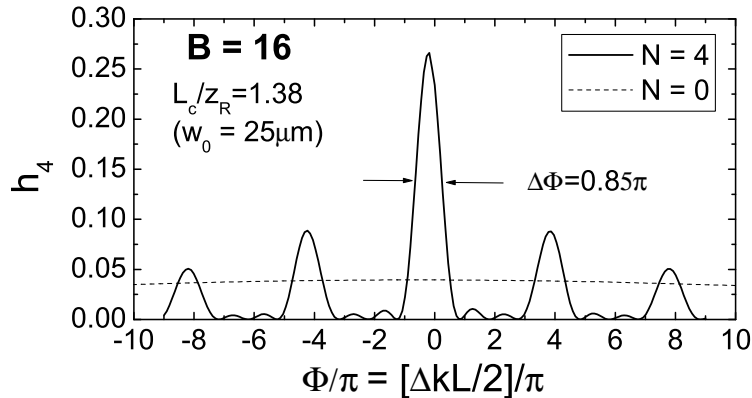


Fig. 7. Theoretical tuning curve of an 8-OCWOC BBO structure ($L_c = 8\text{mm}$), predicting a $7\times$ SH enhancement as compared with a bulk sample.

Fig. 7 plots for instance the tuning curve of an ideal 8-OCWOC structure of the same length $L_c = 8\text{mm}$, showing sideband peaks located at $\Phi/\pi = \pm kN$ ($k = 1, 2, \dots$) in addition to the central lobe whose width is similar to the $N = 1$ case (Fig. 2). The envelope of these side peaks coincides with the individual

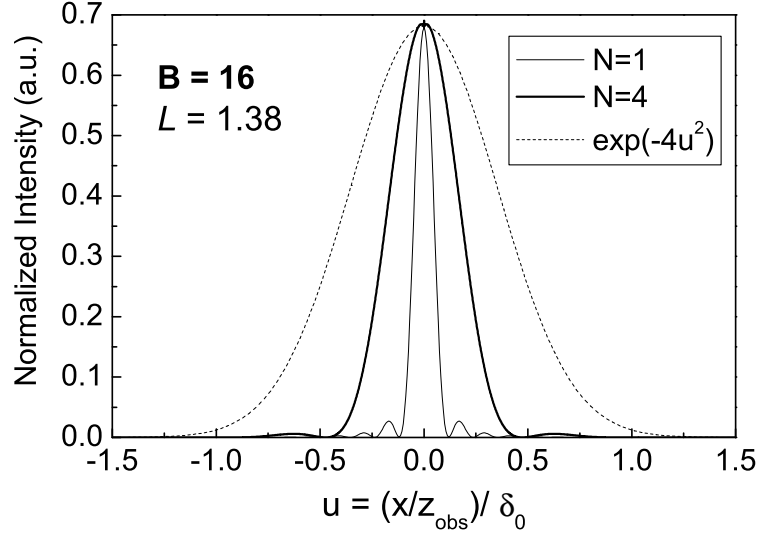


Fig. 8. Transverse far-field pattern of an 8-OCWOC structure ($N = 4$ as compared with that of the 2-OCWOC ($N=1$)). The dashed curve corresponds to the unaffected vertical transverse direction.

plate acceptance bandwidth. An enhancement factor of $\sim 7\times$ compared to a bulk crystal (dashed line) is expected on the main central lobe. Note that significant transmission also exists for 4 adjacent wavelengths, owing to the ideal filter response of the structure. Actually – and hopefully – small residual random fluctuations $\delta\theta_{\text{cut}}(j)$ of plate orientation mismatches washing out the wavevector mismatch grating of the ideal structure will effectively broaden the central lobe [16] to a few times the bandwidth of the bulk equivalent crystal, as already observed with a 10-OCWOC KTP structure [20]. Depending on how far the structure departs from the ideal case, the peaks will be more or less washed out to yield a broad transmission pattern. In the limiting case of large fluctuations [16], the bandwidth of the $2N$ -OCWOC structure may broaden up to that of the individual thin plate. This broadening is however paid back by a reduction of the peak efficiency enhancement.

Finally, we plot in Fig.8 the expected gain in UV beam shape quality, as compared with the simple 2-plate tandem. One notices that the fine oscillatory structure at the wings of the 2-plate tandem has disappeared. Although the profile re-symmetrization is not complete, the UV beam shape ellipticity is drastically reduced, allowing standard beam shaping optics to perform the final re-circularization.

7 Conclusions

In summary, we have performed preliminary investigations of the feasibility of monolithic BBO walk-off compensating structures for deep UV generation.

The preliminary results obtained with a tandem of 2 crystals pledge for the increase of the number of plates with millimeter to sub-millimeter thickness. An increased number of thinner plates should circumvent the accuracy limitations of the fabrication process, increase further the efficiency enhancement and reduce the ellipticity of the UV second-harmonic beam. The experimental behavior of the 2-OCWOC device was found to closely match the expectations derived from the general theory of $2N$ -OCWOC devices inasmuch as SH efficiency enhancement and beam profile improvement are considered.

Due to the lack of more efficient, deep UV transmitting borate materials and to the deep UV high absorption loss of QPM ferroelectrics, $2N$ -OCWOC structures made from BBO inside enhancement resonators open up the prospect of building powerful cw sources with improved beam quality in the deep UV at any wavelength above ~ 200 nm for quantum optics experiments. Our next goal is to demonstrate with a multi-plate monolithic structure sub-watt-level deep UV sources for the efficient cooling and trapping of magnesium and silver atoms from a thermal beam. For each specific targeted wavelength, a preliminary stringent experimental determination of the exact phase-matching angle would be required prior to the design of the appropriate $2N$ -OCWOC structure. Although most useful for the design of cw laser sources, these periodic devices should also prove useful in other BBO-based parametric generation techniques such as chirped-pulse amplification of ultra-short pulses (OPCPA), minimizing spectral phase distortion owing to the $(\pm\Delta k)$ wavevector periodic grating stemming from the walkoff-compensated arrangement [32] and enhancing the gain bandwidth of the amplification process.

References

- [1] J. L. Hall, M. Zhu, P. Buch, J. Opt. Soc. Am. B **6** (1989) 2194.
- [2] G. Uhlenberg, J. Dirscherl, H. Walther, Phys. Rev. A **62** (2000) 063404.
- [3] T. Badr, Y. Louyer, M.D. Plimmer, P. Juncar, D.J.E. Knight, M.E. Himbert, *First observation by two-photon laser spectroscopy of the $4d^{10}5s\ ^2S_{1/2} \rightarrow 4d^95s^2\ ^2D_{5/2}$ transition in atomic silver*, submitted to Eur. Phys. J. D.
- [4] H.J. Metcalf, P. van der Straten, *Laser Cooling and Trapping*, Springer, ed., 2nd ed. (2002).
- [5] N. Beverini, S. De Pascalis, E. Maccioni, D. Pereira, F. Strumia, G. Vissani, Y.Z. Wang, C. Novero, Opt. Lett. **14** (1989) 350.
- [6] J.A. Armstrong, N. Bloembergen, J. Ducuing, P. Pershan, Phys. Rev. **127** (1962) 1018.
- [7] M.M. Fejer, G.A. Magel, D.H. Jundt, R.L. Byer, IEEE J. Quantum Electron. **28** (1992) 2631.

- [8] L.E. Meyers, R.C. Eckardt, M.M. Fejer, R.L. Byer, W.R. Bosenberg, J.W. Pierce, *J. Opt. Soc. Am. B* **12** (1995) 2102.
- [9] A.L. Alexandrovski, G. Foulon, L.E. Meyers, R.K. Route, M.M. Fejer, *Proc. SPIE* **3610** (1999) 44.
- [10] D.N. Nikogosyan, in *Nonlinear optical crystals: A complete survey*, Springer ed., (2005).
- [11] F.T. Goudarzi, E. Riis, *Opt. Commun.* **227** (2003) 389.
- [12] R. Le Targat, J.-J. Zondy, P. Lemonde, *Opt. Commun.* **247** (2005) 471.
- [13] J.-P. Meyen, M.M. Fejer, *Opt. Lett.* **22** (1997) 1214.
- [14] J. Sakuma, Y. Asakawa, M. Obara, *Opt. Lett.* **29** (2004) 92.
- [15] H. Hellwig, J. Liebertz, L. Bohaty, *Solid State Commun.* **109** (1999) 249.
- [16] J.-J. Zondy, Ch. Bonnin, D. Lupinski, *J. Opt. Soc. Am. B* **20** (2003) 1675.
- [17] J.-J. Zondy, M. Abed, S. Khodja, *J. Opt. Soc. Am. B* **11** (1994) 2368.
- [18] D.J. Armstrong, W.J. Alford, T.D. Raymond, A.V. Smith, M.S. Bowers, *J. Opt. Soc. Am. B* **14** (1997) 460.
- [19] A.V. Smith, D.J. Armstrong, W.J. Alford, *J. Opt. Soc. Am. B* **15** (1998) 122.
- [20] J.-J. Zondy, D. Kolker, Ch. Bonnin, D. Lupinski, *J. Opt. Soc. Am. B* **20** (2003) 1695.
- [21] J.-J. Zondy, M. Abed, S. Khodja, C. Bonnin, B. Rainaud, H. Albrecht, D. Lupinski, *Proc. SPIE* **2700** (1996) 66.
- [22] J.P. Fève, J.-J. Zondy, B. Boulanger, R. Bonnenberger, X. Cabirol, B. Ménaert, G. Marnier, *Opt. Commun.* **161** (1999) 359 .
- [23] B.G. Klappauf, Y. Bidel, D. Wilkowski, T. Chanelire, R. Kaiser, *Appl. Opt.* **43** (2004) 2510.
- [24] G.D. Boyd, D.A. Kleinman, *J. Appl. Phys.* **39**(1968) 3597.
- [25] J.-J. Zondy, *Opt. Commun.* **81** (1991) 427.
- [26] L.I. Isaenko, A. Dragomir, J.G. McInerney, D.N. Nikogosyan, *Opt. Commun.* **198** (2001) 433.
- [27] A. Dragomir, J.G. McInerney, D.N. Nikogosyan, *Appl. Opt.* **41** (2002) 4365.
- [28] I. Shoji, H. Nakamura, K. Ohdaira, T. Kondo, R. Ito, T. Okamoto, K. Tatsuki, S. Kubota, *J. Opt. Soc. Am. B* **16** (1999) 620.
- [29] D. Eimerl, L. Davis, S. Velsko, E.K. Graham, A. Zalkin, *J. Appl. Phys.* **62** (1987) 1968.

- [30] S. Carrasco, D.V. Petrov, J.P. Torres, L. Torner, H. Kim, G. Stegeman, J.-J. Zondy, *Opt. Lett.* **29** (2004) 382.
- [31] R.F. Wu, P.B. Phua, K.S. Lai, Y.L. Lim, E. Lau, A. Chang, C. Bonnin, and D. Lupinski, *Opt. Lett.* **25** (2000) 1460.
- [32] I.N. Ross, P. Matousek, G.H.C. New, K. Osvay, *J. Opt. Soc. Am. B* **19** (2002) 2945.